Clinical Neurophysiology 168 (2024) 178–192

Contents lists available at ScienceDirect

Clinical Neurophysiology

journal homepage: www.elsevier.com/locate/clinph

The part and the whole: how single nodes contribute to large-scale phase-locking in functional EEG networks

Anaïs Espinoso [a,*], Marc G. Leguia [a], Christian Rummel [b,c], Kaspar Schindler [d], Ralph G. Andrzejak [a]

[a] Department of Information and Communications Technologies, Universitat Pompeu Fabra, Carrer Roc Boronat 138, Barcelona 08018, Catalonia, Spain
[b] Support Center for Advanced Neuroimaging, University Institute for Diagnostic and Interventional Neuroradiology, Inselspital, Bern University Hospital, University of Bern, Bern, Switzerland
[c] European Campus Rottal-Inn, Technische Hochschule Deggendorf, Max-Breiherr-Strasse 32, D-84347 Pfarrkirchen, Germany
[d] Sleep-Wake-Epilepsy-Center, Department of Neurology, Inselspital, Bern University Hospital, University of Bern, Bern, Switzerland

HIGHLIGHTS

- We study large-scale phase-locking of functional EEG networks and how nodes contribute to it.
- Seizure onset zone nodes increase the phase-locking, while those outside this zone decrease it.
- The seizure onset zone stands out most in a joint analysis of low and high frequencies.

ARTICLE INFO

Article history:
Accepted 13 September 2024
Available online 19 September 2024

Keywords:
Epilepsy
Quantitative electroencephalography
Seizure onset zone
Presurgical epilepsy diagnostics
Synchronization
Seizure networks

ABSTRACT

Objective: The application of signal analysis techniques to electroencephalographic (EEG) recordings from epilepsy patients shows that epilepsy involves not only altered neuronal synchronization but also the reorganization of functional EEG networks. This study aims to assess the large-scale phase-locking of such functional networks and how individual network nodes contribute to this collective dynamics.
Methods: We analyze the EEG recorded before, during and after seizures from sixteen patients with pharmacoresistant focal-onset epilepsy. The data is filtered to low (4–30 Hz) and high (80–150 Hz) frequencies. We define the multivariate phase-locking measure and the univariate phase-locking contribution measure. Surrogate signals are used to estimate baseline results expected under the null hypothesis that the EEG is a correlated linear stochastic process.
Results: On average, nodes from inside and outside the seizure onset zone (SOZ) increase and decrease, respectively, the large-scale phase-locking. This difference becomes most evident in a joint analysis of low and high frequencies.
Conclusions: Nodes inside and outside the SOZ play opposite roles for the large-scale phase-locking in functional EEG network in epilepsy patients.
Significance: The application of the phase-locking contribution measure to EEG recordings from epilepsy patients can potentially help in localizing the SOZ.

1. Introduction

Epilepsy surgery is a potential therapy for patients who suffer from pharmacoresistant focal-onset epilepsy, where seizures originate from a well-defined brain area, the so-called seizure onset zone (SOZ) (Carreno and Lüders, 2008; Rosenow and Lüders, 2001). For some patients, the use of intracranial multichannel electroencephalography (EEG) recordings remains crucial to localize the SOZ precisely. Visual inspection of these recordings along with the application of quantitative EEG signal analysis is used to delineate the SOZ. Seizure freedom after surgery varies from 40 % to 80 % in temporal lobe epilepsy (Spencer and Huh (2008) and references therein) and 40 % to 60 % in extratemporal lobe epilepsy (Krucoff et al. (2017)). An important role in both visual and quantitative EEG analysis is played by recordings of epileptic seizures. Seizures are often considered as a manifestation of abnormal excessive and hypersynchronous neuronal activity (Penfield and Jasper (1954); Fisher et al. (2005)). Classically, neuronal

* Corresponding author.
E-mail address: anais.espinoso@gmail.com (A. Espinoso).

https://doi.org/10.1016/j.clinph.2024.09.008
1388-2457/

synchronization is studied using functional connectivity measures from quantitative EEG analysis (e.g. Brazier (1972); Osterhage et al. (2007); Pijn et al. (1990); Wendling et al. (2001); Lachaux et al. (1999); Mormann et al. (2000); Stam et al. (2007); Ortega et al. (2008); Staniek and Lehnertz (2008); Korzeniewska et al. (2014); Espinoso and Andrzejak (2022); Andrzejak et al. (2011); Mormann et al. (2003)). However, previous studies showed that epileptic seizures, apart from being considered as a manifestation of hypersynchrony, can also be characterized by a network reorganization (Kramer et al. (2010); Schindler et al. (2008); Ponten et al. (2007); Kramer et al. (2008)).

Most studies applying quantitative EEG signal analysis measures just aim at localizing the SOZ and do not consider how the different brain areas interact when the seizure activity spreads (Khambhati et al. (2015)). To analyze these interactions, we can conceptualize the brain as a network, which is composed of nodes and edges (Bullmore and Sporns (2009); Boccaletti et al. (2006)). The nodes of this network are brain areas. The dynamics of individual nodes can be captured by signals, recorded for example by individual channels of an EEG. The edges represent the connections between these nodes, which can be structural via synapses and dendrites or functional as assessed by statistical relations between signals measured from the nodes. There are various graph theory measures used to understand the organization of networks, including measures of the node degree, clustering coefficient and average path length (Bullmore and Sporns (2009); Boccaletti et al. (2006)). Indeed, network analysis can help to understand the organization of brain networks (Bullmore and Sporns (2009); Boccaletti et al. (2006)) and more specifically, in the study of EEG seizure dynamics (Kramer and Cash (2012); Lehnertz et al. (2014); Spencer (2002); van Diessen et al. (2013); Schindler et al. (2008); Burns et al. (2014)). For instance, Burns et al. found that the SOZ is isolated from other brain areas at seizure onset but becomes more connected once the seizure ends (Burns et al. (2014)). According to Kramer and Cash, during seizure propagation the network is more regular and then becomes more random once seizure termination approaches (Kramer and Cash (2012)). Sinha et al. discussed the concept of an aberrant network, which is associated with epileptogenesis and ictogenesis and is patient-specific (Sinha et al. (2022)). Beyond understanding the network topology as a whole, it is important to assess how a specific node affects the entire network. To quantify the contribution of individual nodes to network synchrony, we can estimate the synchronization of a "lesioned" network (Bullmore and Sporns (2009)). Previous studies deleted nodes or edges in model systems to investigate how network synchronization is re-organized, and the network's robustness under certain types of damage (Honey and Sporns (2008); Achard et al. (2006); Kaiser et al. (2007); Bröhl and Lehnertz (2023)).

In this study we address the following main questions. To what degree do the dynamics of the SOZ contribute to the whole network's phase-locking? To what degree do the dynamics of the non-SOZ contribute? How does these phase-locking contributions evolve before, during, and after seizure? To address these questions we apply phase-based synchronization measures combined with surrogates to peri-ictal multichannel EEG recordings. First, we extract the instantaneous phase from each EEG signal using the *analytic signal concept* based on the Hilbert transform (Gabor (1946)). We then determine the multivariate measure of the renormalized mean resultant length (Andrzejak et al. (2023)). It allows us to quantify the degree of large-scale phase-locking across nodes captured by multichannel EEG recordings. To quantify the impact of a specific node on the network, we then compare the phase-locking from the complete network to the one of a reduced network. The complete network is represented by all signals in a multichannel EEG recording. The reduced network is obtained by excluding the channel of the node for which the impact is quantified. The phase-locking contribution measure is then straightforwardly defined by taking the difference between the phase-locking from the complete network and the reduced network. We then use multivariate surrogate signals which allow testing the null hypothesis that the EEG dynamics are a linear stochastic stationary correlated process (Casdagli et al. (1997); Andrzejak et al. (2001); Pijn et al. (1991)). We perform two one-sided surrogate tests to determine if the phase-locking contribution results for the EEG are either below or above the values which are expected under this null hypothesis.

When using phase-based synchronization measures, one has to keep in mind that instantaneous Hilbert phases are not well-defined for broad-band signals (Quian Quiroga et al. (2002)). Indeed, to distinguish between the SOZ and other brain areas based on the mean phase coherence (Mormann et al. (2000)), bandpass filtered signals are better suited (Espinoso and Andrzejak (2022)). To motivate the specific frequency bands analyzed here (Bandarabadi et al. (2019)), we at first recall that high-frequency oscillations (HFOs, >80 Hz) have been demonstrated to be a potential biomarker of the SOZ, as they are involved in seizure initiation (Zijlmans et al. (2012)). In fact, resection of HFOs-generating tissue is associated with good surgical outcomes (Alarcon et al. (1995); Jacobs et al. (2010)). These fast activities not only occur during seizures but also in the same channels during interictal intervals (Zijlmans et al. (2012)). Low frequency oscillations (LFOs, <30 Hz) also play an important role in the initiation of seizures since they can facilitate the communication of different brain areas (Guirgis et al. (2015)). Instead of studying synchronization in separated frequencies, recent work focused on the interactions between HFOs and LFOs. Guirgis et al. studied how the amplitude of a higher frequency is modulated by the phase of a lower frequency (Guirgis et al. (2015)). They found that this cross-frequency coupling provides a more precise localization of the seizure onset zone, which is in agreement with other studies using these techniques (Weiss et al. (2015); Bandarabadi et al. (2019)). Other researchers studied the coexistence of LFOs and HFOs (Modur et al. (2012); Wu et al. (2014); Imamura et al. (2011)), where slow shifts and HFOs are only observed in the SOZ. Here, we investigate the phase-locking contribution in low and high frequencies separately. Additionally, we analyze if the influence of each node on the network phase-locking is consistent across HFOs and LFOs. To this end, we investigate the outcomes of the surrogate tests separately in low and high frequencies and then combine the results in a joint test across both frequency ranges.

2. Materials and methods

The MATLAB source codes used in this study are publicly available at Ref. Espinoso et al. (2024).

2.1. Database

We use a database composed of intracranial EEG recordings from sixteen patients (11 females, median age 31 yo, range 19–59 yo) suffering from focal-onset pharmacoresistant epilepsy (Rummel et al. (2015)). The recordings were acquired as part of the presurgical evaluation at the Inselspital Bern (Switzerland). Clinicians located the seizure onset zone in one of the hemispheres, and all patients underwent epilepsy surgery. The surgical outcome was evaluated during several years after the surgery, classifying the patients according to the Engel Epilepsy Surgery Outcome Scale (Engel Jr (1993)). This database was previously studied in Refs. Rummel et al. (2015); Goodfellow et al. (2016); Bandarabadi et al. (2019); Burrello et al. (2020). This study was approved by

the Ethics committee of the Canton of Bern (approval No. 2017–00697).

As explained in detail in Ref. Rummel et al. (2015), the visual inspection of these EEG recordings was performed by a board-certified epileptologist (K.S.). The time instants of seizure onset and termination were determined for all seizures along with the SOZ channels, i.e. the channels where the first seizure EEG signal changes could be detected. The remaining nonSOZ channels were recorded from brain areas that were not involved in the seizure at its onset. Each recording includes three minutes immediately before seizure onset, the seizure of variable duration, and three minutes after seizure termination. Fig. 1 shows an example of such a recording.

Table 1 shows the demographic and clinical information of the patients included in this study. The number of recorded seizures varied across patients. To not over-represent the patients with more recorded seizures in the analysis, only two seizures of each patient are included, which is the minimum number found across the patients (Table 1) (Rummel et al. (2015); Bandarabadi et al. (2019)). To select the two seizures for patients having more registered seizures, we use the pathway dissimilarity method presented in Refs. Schroeder et al. (2020); Schroeder et al. (2022). This method quantifies the degree of dissimilarity between seizure pathways, as determined by the temporal evolution of their functional connectivity matrices. We select the two seizures with the highest dissimilarity value for our analysis to ensure maximal diversity among seizures. Details and results of the pathway dissimilarity method are shown in the Supplementary Material. The average duration of all seizures included in the analysis is 145.3 ± 37.1 s.

2.1.1. Preprocessing

The data were at first filtered using a fourth-order Butterworth band-pass filter between 0.5 and 150 Hz and sampled at 512 Hz. The signals were re-referenced against the median of all channels free of permanent artifacts (Rummel et al. (2007)). For the evaluation of LFOs and HFOs, we follow Ref. Bandarabadi et al. (2019) and use two additional filtering settings. A finite impulse response (FIR) band-pass filter is applied between 4 and 30 Hz for the analysis of lower frequencies and between 80 and 150 Hz for higher frequencies. For all subsequent steps of analysis, we use a moving window w of 20 s, resulting in $N = 10240$ samples per window, with a 75% overlap between subsequent windows. We excluded 2.88% of all time windows across all channels and 0.69% of all channels across all time windows due to prominent artifacts identified by visual inspection.

2.2. Multivariate phase-locking

To quantify the large-scale phase-locking of the brain network, we use the temporal average of the re-normalized mean resultant length (Andrzejak et al. (2023)). Because a complete derivation of this measure is quite lengthy, we restrict ourselves to the aspects which are most relevant for our context. We only provide the measure's definition in Eq. (1) and describe its main features and advantages. How this approach is embedded in circular statistics (Mardia and Jupp (2000)) and how it is connected to well-known measures like the Kuramoto order parameter (Kuramoto (1984)) or the phase-locking value (Lachaux et al. (1999)) is described in Ref. Andrzejak et al. (2023).

Suppose we have a window of an EEG recording with s channels. This data provides s signals consisting of N samples each taken at discrete times t_j for $j = 1, \ldots, N$. Here, t_1 and t_N correspond to the beginning and end of the window w, respectively. Recall that each signal represents the dynamics of one network node covered by the corresponding recording channel. We at first extract the instantaneous phase $\varphi_k(t_j)$ from each signal for $k = 1, \ldots, s$ using the *analytic signal concept* based on the Hilbert transform (Gabor (1946)). It is important to note that this instantaneous phase is conceptually different from the phases of Fourier coefficients for each frequency. The phase $\varphi_k(t_j)$ maps the momentary state of node k at every time instant t_j to a value between 0 and 2π. It takes into account all frequencies contained in the Fourier spectrum of the underlying signal. Accordingly, in contrast to phases of Fourier coefficients, the instantaneous phase is time resolved and reflects the dynamics across more than one single frequency.

Given the instantaneous phase $\varphi_k(t_j)$ of the s channels for the times t_j included in window w, we use the temporal average of the re-normalized mean resultant length (Andrzejak et al. (2023)) to determine the multivariate phase-locking:

$$\zeta(\varphi_1, \ldots, \varphi_k, w) = \left\langle \frac{\left| \sum_{k=1}^{s} e^{i\varphi_k(t_j)} \right| - \frac{1}{2}\sqrt{\frac{\pi}{s}}}{1 - \frac{1}{2}\sqrt{\frac{\pi}{s}}} \right\rangle_{t_j \in w} . \quad (1)$$

Here i is the imaginary unit in the complex plane, $|\cdot|$ is the vector length in the complex plane, and $\langle\cdot\rangle$ denotes the average across the time interval indicated in the index. We get the maximal degree of multivariate phase-locking if all s phases evolve identically during the entire time in w. In other words, the $\varphi_k(t_j)$ change with time, but $\varphi_1(t_j) = \varphi_2(t_j) = \ldots \varphi_k(t_j)$ for all $t_j \in w$. In this limit $\zeta(\varphi_1, \ldots, \varphi_k, w)$ attains its upper bound one. In the other limit of a complete lack of phase-locking, all phases evolve independently over time and $\zeta(\varphi_1, \ldots, \varphi_k, w)$ has an expected value of zero. The decisive advantage of using the re-normalized mean resultant length in definition Eq. (1) is that this expected value of zero is obtained regardless of the number of channels s. Using the original mean resultant length would lead to a non-zero offset, which could be misinterpreted to indicate some degree of phase-locking. Moreover, the value of this offset would depend on s, and therefore bias would be induced when comparing the multivariate phase-locking across different s. We can therefore use Eq. (1) to compare the multivariate phase-locking across networks with different numbers of nodes which is crucial for the steps of analysis described in the subsequent subsection.

2.3. Phase-locking contribution measure

To quantify the contribution of individual nodes to the large-scale phase-locking of the whole network, we quantify how the multivariate phase-locking is affected when the node's signal is removed from the set of all signals (see also Ref. Schindler et al. (2010)). Specifically, we remove the signal of one node at a time, resulting in s reduced networks, each assessed by $s - 1$ signals. The contribution of the node m is then determined by the difference between the multivariate phase-locking of the complete network and the network reduced by removing signal m:

$$\delta_m(w) = \zeta(\varphi_1, \ldots, \varphi_s, w) - \zeta_m(\varphi_1, \ldots, \varphi_{m-1}, \varphi_{m+1}, \ldots, \varphi_s, w) \quad (2)$$

If $\delta_m(w) > 0$, the node m increases the large-scale phase-locking of the network, indicating that this node enhances the network's synchronization during the window w. In contrast, $\delta_m(w) < 0$ indicates that the dynamics of this node decreases the overall synchronization. Finally, $\delta_m(w) = 0$, implies that the node m has no impact on the synchronization. We should note that by using $\delta_m(w)$, we derive a set of s univariate phase-locking contribution measures from the multivariate phase-locking of Eq. 1.

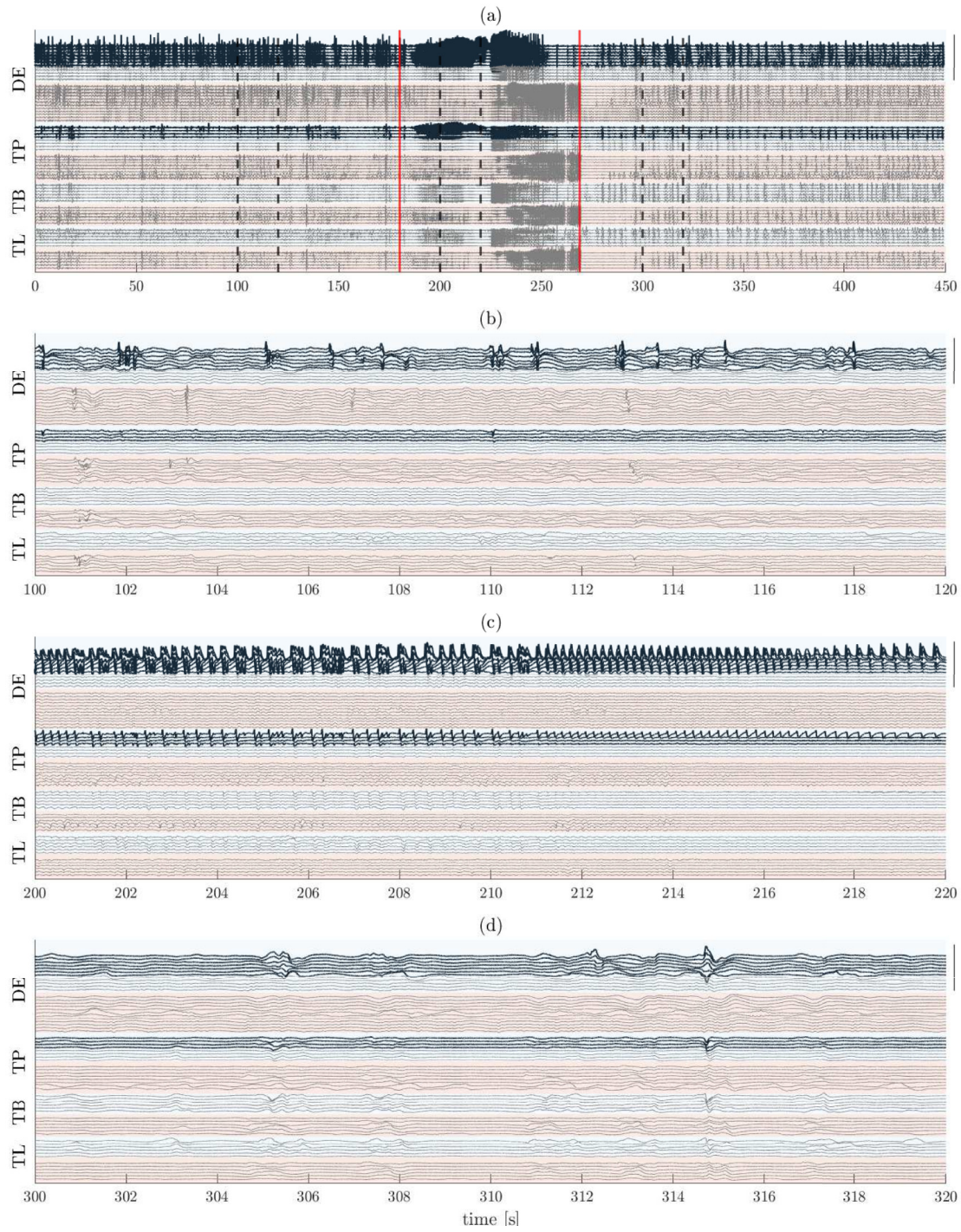

Fig. 1. Exemplary multi-channel EEG signals from the first recorded seizure of patient I-2. The recordings were performed using 4 electrodes for each hemisphere, carrying a total of 64 channels. EEG signals measured with channels located in the right hemisphere (blue background) and in the left hemisphere (orange background) are shown. The signals registered from the SOZ displayed with a greater line width. (a) Entire recording including 180 s before seizure onset, seizure activity which lasted 90 s in this case, and 180 s after seizure termination. The continuous vertical red lines indicate the seizure onset and seizure termination. The vertical dashed black lines indicate the 20 s windows displayed in (b), (c), and (d). (b) Window before seizure onset. (c) Window during the seizure. (d) Window after seizure termination. The vertical black lines at the right part of each panel are all the same length and indicate the EEG amplitudes: 6889 μV, 5794 μV, 5905 μV, and 5857 μV, respectively. Channel labels: DE, depth electrode; TP, temporo-posterior; TB, temporo-basal; TL, temporo-lateral. Results for this exemplary recording are shown in Figs. 2–3.

2.4. Surrogates

The framework of surrogates is a powerful tool in signal analysis that allows testing well-defined null hypotheses about the dynamics underlying some measured signals (Theiler et al. (1992)). The principle of surrogates is straightforward. At first, one analyses the original data, then one randomizes this data to obtain surrogate data. The analysis is then repeated for the surrogate data, and it is tested if the result is different from what was obtained for the original data. In our case, one surrogate data window is given by a randomized version of one window of the EEG recording. Since an EEG recording with s channels provides s

Table 1
Demographic and clinical information of all 16 patients. The patient ID includes the Engel Epilepsy Surgery Outcome Scale: I (completely seizure-free), II (almost seizure-free, still some disabling seizures), and IV (no worthwhile improvement). The second column indicates the age of the patient at surgery. The syndrome stands for the type of epilepsy: FLE (frontal lobe epilepsy), LTLE (lateral temporal lobe epilepsy), MTLE (mesial temporal lobe epilepsy), PLE (parietal lobe epilepsy). The hemisphere denotes the side of the seizure onset zone, either right (R) or left (L). The follow-up indicates the years of post-surgical control. The number of recorded seizures stands for the total number of consecutive seizures recorded for each patient during the pre-surgical diagnostics with intracranial electrodes. The number of electrodes refers to the intracranial electrodes implanted in both hemispheres. The number of channels is the total amount of contacts included in all electrodes. In general, different electrodes have different numbers of channels.

ID	Age at surgery (yo)	Syndrome	Hemisphere	Follow-up (y)	Recorded seizures	Electrodes	Channels
I-1	26	MTLE	R	3	2	10	64
I-2	48	MTLE	L	3	4	8	64
I-3	27	LTLE	L	1	9	7	56
I-4	36	PLE	L	5	7	3	74
I-5	19	MTLE	L	5	4	5	42
I-6	25	FLE	R	4	2	13	98
II-1	49	FLE	R	4	6	12	92
II-2	46	LTLE	R	3	5	12	100
II-3	20	LTLE	R	3	10	7	54
II-4	31	LTLE	L	3	6	10	59
II-5	24	LTLE	L	3	2	6	47
IV-1	38	LTLE	L	4	2	8	59
IV-2	23	LTLE	L	2	3	10	61
IV-3	59	MTLE	L	3	10	7	49
IV-4	32	PLE	L	2	14	14	62
IV-5	31	FLE	R	2	2	6	36

signals, the surrogate also has s signals. The surrogate data window is constructed such that each of its s surrogate signals has the same amplitude distribution and autocorrelation like its corresponding original EEG signal. Moreover, the pairwise cross-correlation between all s signals is maintained. Except for these constraints, the surrogates are constructed to be random. A set of surrogate data windows is obtained from independent realizations of the randomization process. To generate these surrogates we use the multivariate *iterative amplitude adjusted Fourier transform* (IAAFT) algorithm (Schreiber and Schmitz (1996)). This type of surrogates can be used to numerically estimate values of $\delta_m(w)$ expected under the null hypothesis H_0: The signals are generated by a multivariate stationary linear stochastic auto- and cross-correlated Gaussian process. The amplitude distribution of the original signals is preserved in the surrogates to account for possible nonlinearities in the measurement functions Prichard and Theiler (1994); Schreiber and Schmitz (2000); Andrzejak et al. (2012).

2.5. Null hypothesis tests and outcomes

In this subsection, we describe the surrogate based test of the null hypothesis H_0, which we denote by $\mathscr{D}$. Given the w-th window of an EEG recording, we calculate the phase-locking contribution measure for each of the s original signals. We denote this by $\delta_{m,\mathrm{orig}}(w)$, where $m = 1, \ldots, s$. This procedure is repeated for each of 19 surrogate data windows, yielding a set of 19 values $\{\delta_{m,\mathrm{surr}}(w)\}$. The test $\mathscr{D}$ can have three different outcomes, depending on where the value $\delta_{m,\mathrm{orig}}(w)$ is located with respect to the distribution obtained for the surrogates $\{\delta_{m,\mathrm{surr}}(w)\}$. We denote as outcome A if $\delta_{m,\mathrm{orig}}(w)$ is higher than the maximum value in the set $\{\delta_{m,\mathrm{surr}}(w)\}$. Outcome B is obtained if $\delta_{m,\mathrm{orig}}(w)$ is lower than the minimum value in $\{\delta_{m,\mathrm{surr}}(w)\}$. Finally, if $\delta_{m,\mathrm{orig}}(w)$ is within the distribution of values in $\{\delta_{m,\mathrm{surr}}(w)\}$, we get outcome C. Formally, outcome A and B represent the rejection of the two complementary one-sided tests of H_0. Usually, one of the one-sided hypothesis tests is selected *a priori* (Refs. Andrzejak et al. (2012); Andrzejak et al. (2003)) or surrogate results are used as a baseline for the signal analysis measures (Ref. Andrzejak et al. (2011)). Instead, we apply here both one-sided surrogate tests by considering both outcome A and B. Both one-sided tests have a significance level of 0.05. Accordingly, if H_0 was true we would expect approximately 5% of outcome A, 5% of outcome B, and 90% of outcome C across all windows and channels, if we assume that results are independent across windows and channels.

We use the two filter settings presented in Section 2.1.1. To distinguish between both settings we add a subindex to the null hypothesis test symbol, i.e., $\mathscr{D}_L$, when applying the test to the signals filtered to the low-frequency band (4–30 Hz), and $\mathscr{D}_H$, when applying the test to the signals filtered to the high-frequency band (80–150 Hz). Moreover, we perform a joint test denoted as $\mathscr{D}_J$. If both tests $\mathscr{D}_L$ and $\mathscr{D}_H$ have outcome A, the test $\mathscr{D}_J$ is said to have outcome A as well. In analogy, $\mathscr{D}_J$ is said to have outcome B, if both $\mathscr{D}_L$ and $\mathscr{D}_H$ have outcome B. In all other cases, the test $\mathscr{D}_J$ has outcome C. Recall that since we use 19 surrogate data windows jointly with the original EEG window, the significance level $\alpha_{L,H}$ for tests $\mathscr{D}_L$ and $\mathscr{D}_H$ is 0.05 for both outcomes A and B. Under the assumption that the tests for low and high frequencies are independent, the significance level α_J of the joint test $\mathscr{D}_J$ is 0.0025.

The following steps are used to quantify the degree to which a certain outcome of the tests is obtained more often for signals from SOZ or nonSOZ channels. Let $\langle p_{L,\mathrm{A}}^{\mathrm{SOZ}} \rangle_b$ and $\langle p_{L,\mathrm{A}}^{\mathrm{nonSOZ}} \rangle_b$ denote the fraction with which outcome A is obtained for test $\mathscr{D}_L$ across all time windows included in the period before the seizure and across all SOZ and nonSOZ channels, respectively. From this, we define the relative difference:

$$\lambda_{L,\mathrm{A}}^{\mathrm{b}} = \frac{\langle p_{L,\mathrm{A}}^{\mathrm{SOZ}} \rangle_b - \langle p_{L,\mathrm{A}}^{\mathrm{nonSOZ}} \rangle_b}{\langle p_{L,\mathrm{A}}^{\mathrm{SOZ}} \rangle_b + \langle p_{L,\mathrm{A}}^{\mathrm{nonSOZ}} \rangle_b} \tag{3}$$

The values $\lambda_{L,\mathrm{A}}^{\mathrm{b}}$ are bounded in [-1,1]. Positive values indicate that outcome A is more frequent for SOZ channels than for nonSOZ channels. The upper limit of $\lambda_{L,\mathrm{A}}^{\mathrm{b}} = 1$ is found if outcome A is found only for SOZ and not at all for nonSOZ channels. In complete analogy, negative values of $\lambda_{L,\mathrm{A}}^{\mathrm{b}}$ indicate that outcome A is less frequent for SOZ channels than for nonSOZ channels. The lower limit of $\lambda_{L,\mathrm{A}}^{\mathrm{b}} = -1$ is found if outcome A is found only for nonSOZ and not at all for SOZ channels. If the fraction of outcome A is the same for SOZ and nonSOZ, we get $\lambda_{L,\mathrm{A}}^{\mathrm{b}} = 0$. Analogous quantities are defined for the outcome B, the other tests $\mathscr{D}_H$ and $\mathscr{D}_J$, and for the periods during (d) and after (a) the seizure. We do not determine relative differences for outcome C. Whenever we refer to the relative differences in general, we drop the indices specifying the tests, outcomes, and periods, resulting in the simplified notation λ.

3. Results

3.1. Detailed results for an exemplary patient

We at first show detailed results for one exemplary seizure (Figs. 2,3). For this purpose, we use the first registered seizure of patient I-2, who belongs to the group of patients who became seizure-free after surgery (see again Fig. 1). For this patient, the SOZ channels are part of the DEL and TPL electrodes. We start with the analysis of the low frequencies (4–30 Hz). We show values of the phase-locking contribution measure $\delta_{m,\mathrm{orig}}(w)$ across channels for individual windows (Fig. 2(a)) and averaged across the windows during the periods before, during, and after the seizure (Figs. 2(b)-(d)). The channel-window profile in Fig. 2(a) shows prominent regions of both positive values and negative values of $\delta_{m,\mathrm{orig}}(w)$. These indicate that the dynamics underlying these channels increase and decrease, respectively, the large-scale phase-locking during the corresponding intervals. The period-wise averages in Figs. 2(b)-(d) show, however, that there are no systematic differences with regard to the SOZ and nonSOZ channels. Channels of both categories have either positive and negative average values.

The tests $\mathscr{D}$ are based on the comparison of the phase-locking contribution measure of the original EEG data windows against a distribution of values obtained for surrogate data windows. Figs. 2(e)-(h) therefore display $\Psi_m(w) = \delta_{m,\mathrm{orig}}(w) - \mu\{\delta_{m,\mathrm{surr}}(w)\}$, where $\mu\{\cdot\}$ denotes the mean across the 19 surrogate results. The largest absolute $\Psi_m(w)$ values and also the strongest variations of this quantity are found in the second half of the seizure and directly after its end (Fig. 2(e)). In particular, for many channels the $\Psi_m(w)$ values switch signs exactly at the end of the seizure. This switching is not obtained for the original values $\delta_{m,\mathrm{orig}}(w)$. This illustrates that $\delta_{m,\mathrm{orig}}(w)$ and $\Psi_m(w)$ can have different signs. To interpret this finding consider the following example. Suppose that

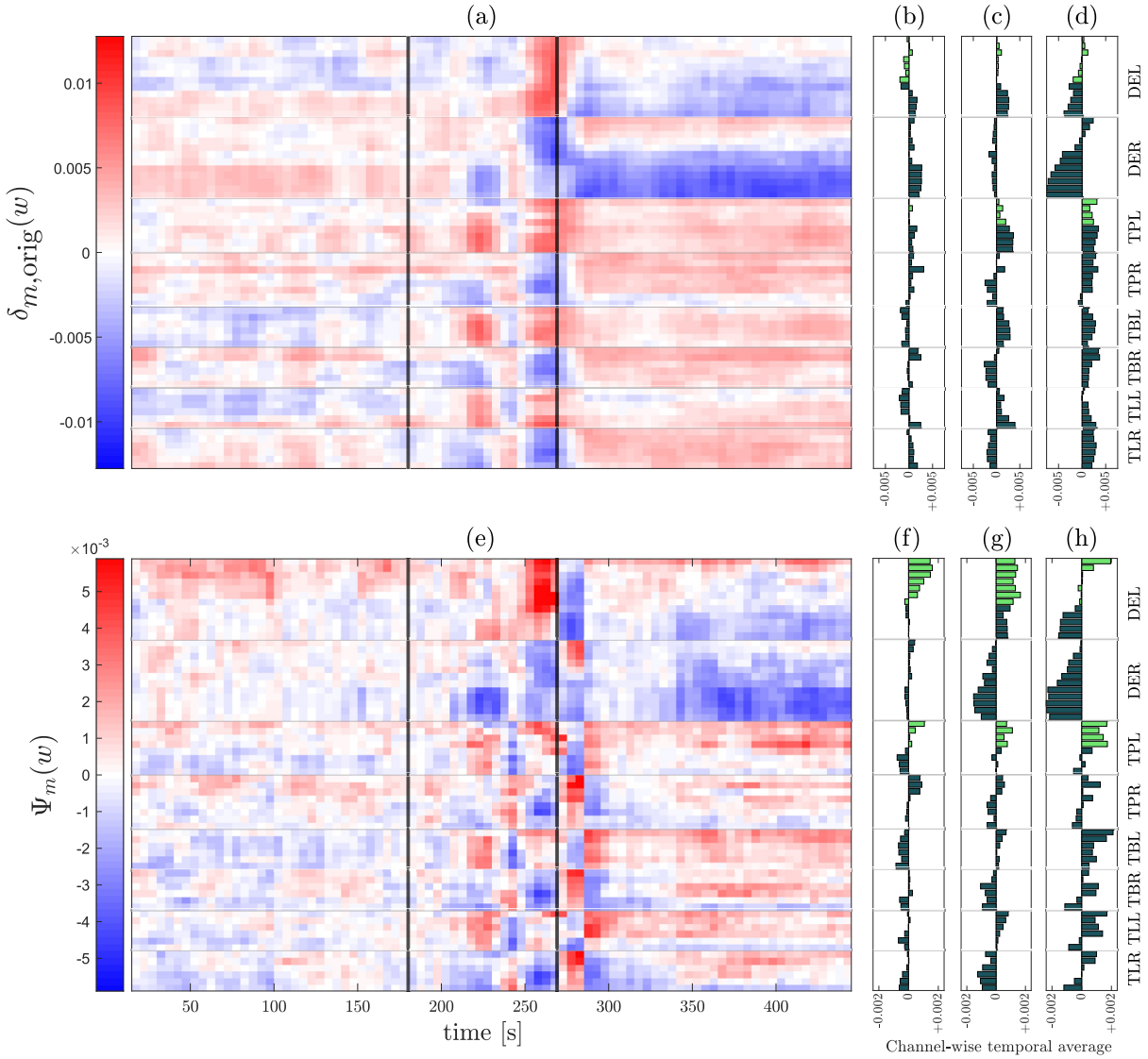

Fig. 2. Higher differences between phase-locking contribution measure for the original EEG signals and surrogate signals are found for SOZ. Values of $\delta_{m,\mathrm{orig}}(w)$ and $\Psi_m(w)$ for different channel categories and periods for the first registered seizure of patient I-2 analysing low frequencies (4–30 Hz). For (a) and (e) vertical black lines indicate the beginning and end of the seizure. For (b), (c), (d), (f), (g), and (h) light and dark green indicate SOZ and nonSOZ channels, respectively. (a) Temporal evolution of $\delta_{m,\mathrm{orig}}(w)$ for all channels. (b) Channel-wise temporal average of values in (a) across the before seizure period. (c) Same as (b) but for the period during the seizure. (d) Same as (b) and (c) but for the period after the seizure. (e) Same as (a) but for $\Psi_m(w)$. (f), (g), and (h) same as (b), (c), and (d), respectively, but showing temporal averages from panel (e). Channel labels are as in Fig. 1: DE, depth electrode; TP, temporo-posterior; TB, temporo-basal; TL, temporo-lateral; but now accompanied by L or R if the electrodes are located in the left or right hemisphere, respectively.

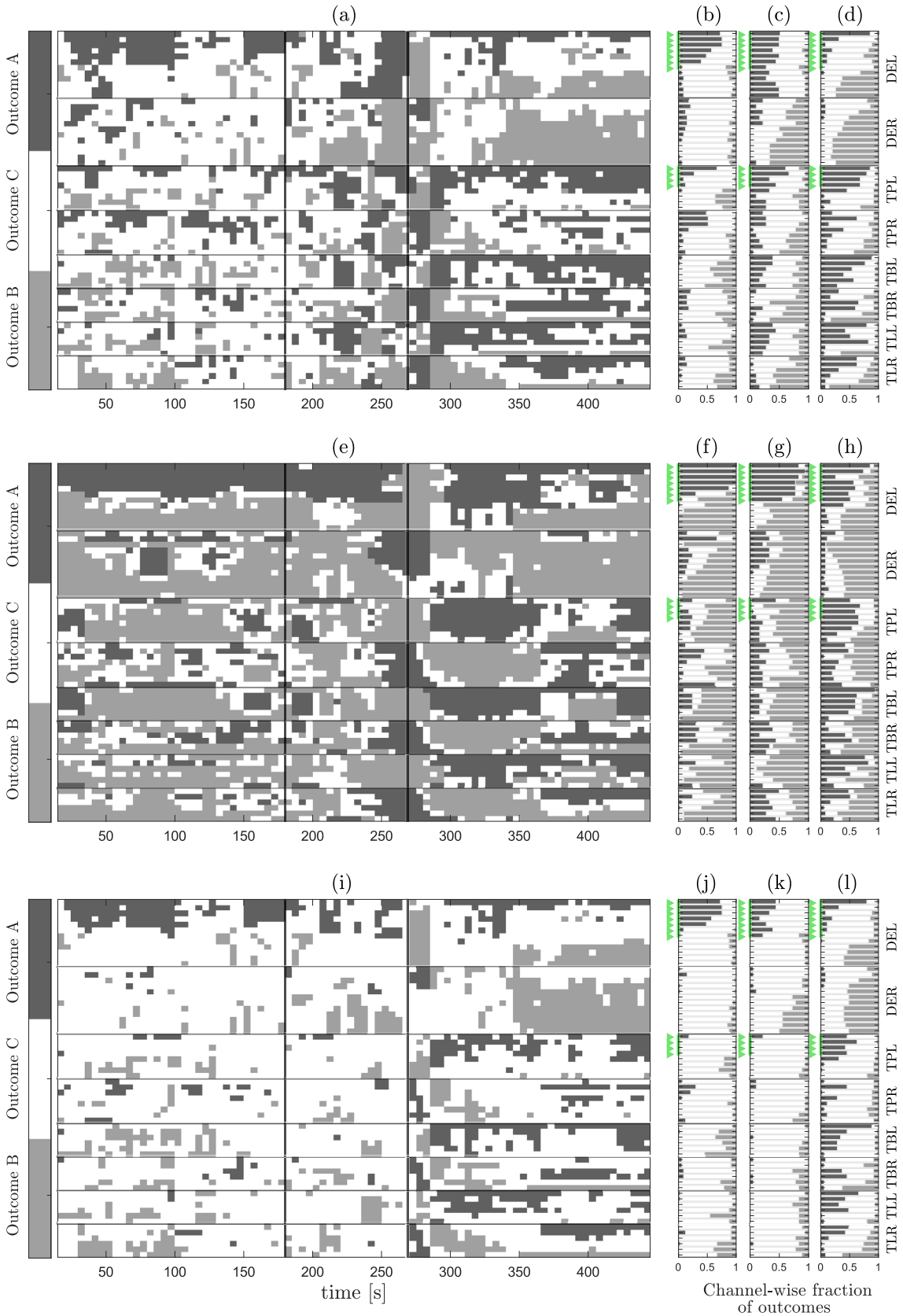

Fig. 3. Signals registered from SOZ and nonSOZ channels show a higher fraction of outcome A and B, respectively, for all tests. Results for the first registered seizure of patient I-2 for the three possible outcomes (A, B, or C) from the surrogate test $\mathscr{D}_L$ (low frequencies (4–30 Hz)). Organization of panels (a)-(d) analogous to (a)-(d) and (e)-(h) in Fig. 2 but here for the outcomes of the test. In panels (b), (c), and (d) we show stacked bar charts with the fraction of outcomes: A, B, and C. (e)-(h) Same as (a)-(d) but showing the outcomes of $\mathscr{D}_H$ (high frequencies (80–150 Hz)). (i)-(l) Same as (a)-(d) but showing the outcomes of $\mathscr{D}_J$ (joined test across high and low frequencies).

$\delta_{m,\mathrm{orig}}(w)$ is positive which implies that for window w the channel m increases to the large-scale phase-locking. However, if $\Psi_m(w)$ is negative, that means that this positive phase-locking contribution stays below what is expected under the surrogates' null hypothesis H_0. This illustrates that the surrogates indeed allow extracting information going beyond the one extracted from the original data. Regarding values of $\Psi_m(w)$ averaged across time for the periods before, during, and after the seizure in Figs. 2(f)-(h) we see that almost all values for the SOZ are positive. Recall that no such clear tendency was found for the average results of the original dynamics $\delta_{m,\mathrm{orig}}(w)$ shown in Figs. 2(b)-(d). For the nonSOZ channels, no clear tendency is found, neither for $\delta_{m,\mathrm{orig}}(w)$ nor for $\Psi_m(w)$.

Results of the tests $\mathscr{D}_L$, which is based on $\delta_{m,\mathrm{orig}}(w)$ and $\{\delta_{m,\mathrm{surr}}(w)\}$ obtained for the signals filtered in low frequencies (4–30 Hz), are shown in Figs. 3(a)-(d). According to the definition of the outcomes, high positive and high negative $\Psi_m(w)$ correspond predominantly to outcome A and B, respectively. For small absolute $\Psi_m(w)$, values of $\delta_{m,\mathrm{orig}}(w)$ mostly remain within the distribution $\{\delta_{m,\mathrm{surr}}(w)\}$, i.e. outcome C is obtained. In the following description, we focus our attention on the outcomes A and B. In the period before the seizure, outcome A is most frequent in the SOZ channels of the electrode DEL. Multiple switching between different outcomes across time can be seen for many channels during the second half of the seizure and directly after its end. Notably, as shown in Fig. 1, the seizure activity spreads to nonSOZ channels of the electrodes DEL, TPL, TBL, and TLL at approximately second 225. It is around that time that these channels show periods of outcome A. Recall that these electrodes were implanted in the left hemisphere which contained the SOZ in this patient. A spread of seizure activity to electrodes DER, TPR, TBR, and TLR in the right hemisphere takes place only later. It is also reflected in a transient increase of outcome A for these electrodes, however to a lesser degree than for DEL, TPL, TBL, and TLL. On the other hand, outcome A is very prominent in the electrodes TPR, TBR, TLR, and some channels of the DER electrode directly after the end of the seizure. Shortly after, more stable patterns arise such as prominence of outcome B in many channels of the electrode DER, to name only one example.

So far we presented results of the first seizure of patient I-2 obtained for the signals filtered in low frequencies (4–30 Hz). We now consider the signals of the same seizure filtered in high frequencies (80–150 Hz) and show outcomes of the corresponding test $\mathscr{D}_H$ in Figs. 3(e)-(h). Overall, there is less outcome C as compared to the results of $\mathscr{D}_L$ (Figs. 3(a)-(d)). Outcome A is most prominent for SOZ channels of the depth electrode DEL throughout the duration of the recording, except for a brief period around the end of the seizure. During this period, outcome B prevails not only in the entire electrode DEL but also in the other electrodes in the left hemisphere. In contrast, at the same period, outcome A dominates in the right electrodes. Interestingly, this pattern switches shortly after the end of the seizure until approximately second 365 where outcome A and B are more frequent in the left and right, respectively.

The joint test $\mathscr{D}_J$ (Figs. 3(i)-(l)) allows us to highlight those periods and channels for which the individual tests $\mathscr{D}_L$ and $\mathscr{D}_H$ for low and high frequencies have the same outcome. By construction, we get an overall higher fraction of outcome C. This is because $\mathscr{D}_J$ has outcome A only if $\mathscr{D}_L$ and $\mathscr{D}_H$ both have outcome A, and it has outcome B only if $\mathscr{D}_L$ and $\mathscr{D}_H$ both have outcome B. In all other cases, it has outcome C. For the SOZ channels belonging to the DEL electrode, outcome A is dominating before and during the seizure, with almost complete absence of outcome B. Directly after the seizure we find outcome B in almost the entire electrode DEL and parts of the other electrodes in the left hemisphere. At the same period, outcome A is found in parts of the right electrodes. After this brief period immediately after the seizure and up until the end of the recording, outcome A and B are more frequent in the left and right electrodes, respectively.

3.2. Distinction between SOZ and nonSOZ channels

We now consider the fractions of the outcomes A, B, and C. We do so for each test ($\mathscr{D}_L$, $\mathscr{D}_H$, and $\mathscr{D}_J$), separately for SOZ and nonSOZ channels, and for each time period (before, during, and after the seizure). Results for the first seizure of patient I-2 are shown in Fig. 4. Overall, outcome A is more prominent in SOZ channels, and outcome B is more prominent in nonSOZ channels. This is consistent across tests and periods. For SOZ channels, outcome A is always more frequent than outcome B, and for nonSOZ channels outcome B is always more frequent than outcome A. Moreover, outcome A is always more frequent in SOZ channels than in nonSOZ channels, and outcome B is always more frequent in nonSOZ channels than in SOZ channels. As a direct consequence, the relative differences λ between SOZ and nonSOZ are positive for outcome A and negative for outcome B, throughout all three tests and all three periods (see Table 2(a)). Accordingly, the results for this example seizure indicate that SOZ nodes enhance the large-scale phase-locking. In contrast, nonSOZ nodes decrease the large-scale phase-locking. Comparing the three tests, the highest absolute value of λ is almost always found for the joint test $\mathscr{D}_J$. The only exception is given by outcome B for the period before the seizure, for which the test based on the low frequencies ($\mathscr{D}_L$) has the maximal absolute λ value. Comparing the three periods, there is no clear tendency since the highest absolute values of λ are generally found for different periods.

Recall that the database used in this study includes EEG recordings from sixteen patients with two seizures analyzed for each patient (See Section 2.1). The fraction of outcomes for the tests $\mathscr{D}_L$, $\mathscr{D}_H$, and $\mathscr{D}_J$ of these thirty-two seizures are averaged and shown in Fig. 5. Overall, Fig. 5 strongly resembles Fig. 4, meaning that the first registered seizure of patient I-2 is a representative example from the group of seizures. This is further supported by the relative differences λ determined from the across-seizure averages of the fractions of outcomes (Table 2(b)). The overall magnitude of the λ is smaller for the across-seizure average than for the example seizure of patient I-2. Nonetheless, throughout all three tests and all three periods, λ values are all positive for outcome A, and all negative for outcome B. That means that the results across seizures further support that SOZ channels and nonSOZ channels increase and decrease, respectively, the large-scale phase-locking. Comparing the three tests, the highest absolute value of λ is now found without exception for the joint test $\mathscr{D}_J$. Comparing the three periods, the highest absolute values of λ are found for the period before the seizure for tests $\mathscr{D}_L$ and $\mathscr{D}_J$, and for the period during the seizure for the test $\mathscr{D}_H$.

So far, we considered the relative differences of outcomes between SOZ and nonSOZ channels (λ) for an individual patient (Table 2(a)) and for the average across all thirty-two seizures from the sixteen patients (Table 2(b)). Fig. 6 shows the λ values for every period, test type, and outcome across all individual seizures. For outcome A, in the majority of the thirty-two cases we get $\lambda > 0$ (Figs. 6(a)-(c)) across all three tests ($\mathscr{D}_L, \mathscr{D}_H$, and $\mathscr{D}_J$) as well as across all three periods (before, during and after the seizure). This is consistent with the positive values in the three first rows in Table 2(b). We have the highest number of instances with $\lambda > 0$ for the period during seizure occurrence. This suggests that in particular during this period, SOZ nodes enhance the network phase-locking. This effect gets weaker after the seizure, where we find up to 12 negative λ values. With regard to outcome B (Figs. 6(d)-(f)), according to the negative values in the last three

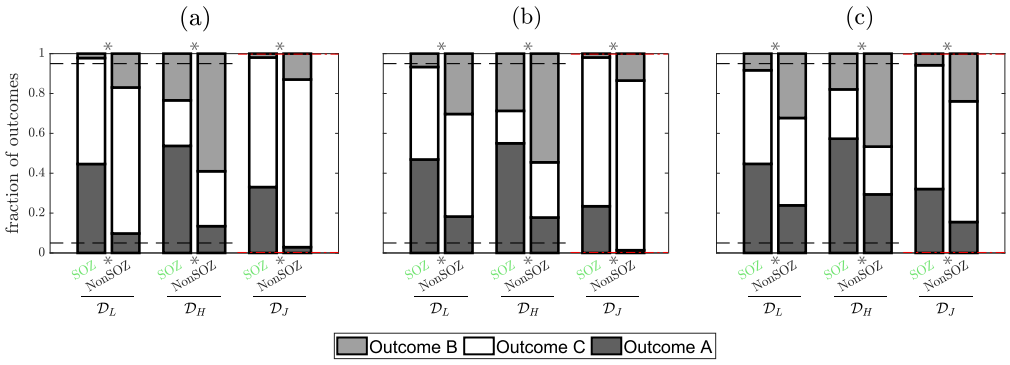

Fig. 4. For the first registered seizure from patient I-2, for all three tests, outcome A is more frequent for SOZ channels, and outcome B is more frequent for nonSOZ channels. Fraction of outcomes A (dark gray), B (light gray), outcome C (white) of the test in low frequencies ($\mathscr{D}_L$), high frequencies ($\mathscr{D}_H$), and the joint test ($\mathscr{D}_J$) for SOZ and nonSOZ channels. (a) Results for the period before seizure onset. (b) Same as (a) but for the period during the seizure. (c) Same as (a) but for the period after the seizure. With the exception of $\langle p_{LB}^{SOZ} \rangle_b$, i.e. the fraction of outcome B of test $\mathscr{D}_L$ for the SOZ channels in the period before the seizure, all fractions of outcomes are above the values to be expected under the null hypothesis H_0. These values are 0.05 for the $\mathscr{D}_L$ and $\mathscr{D}_H$ test (dashed black lines), and 0.0025 for the $\mathscr{D}_J$ test (dashed-dotted red lines). In Table 2(a) we show the corresponding λ values. The asterisks ($*$) indicates p-value < 0.0056. That means the two fractions used to calculate the λ values are significantly different according to a two-proportion z-test (see Chapter 9.4 in Ref. Bluman, 2024) using a Bonferroni correction for 9 comparisons (3 periods and 3 tests) using an initial significance level of 0.05.

Table 2
Relative difference λ (Eq. 3): (a) for the first registered seizure of patient I-2 across all tests ($\mathscr{D}_L$, $\mathscr{D}_H$, and $\mathscr{D}_J$) and for every period (before, during and after seizure occurrence). The values of λ are determined separately for outcome A (first rows) and outcome B (last rows). (b) Analogous to (a) but for all seizures across all patients.

Test		Before	During	After
Outcome A	$\mathscr{D}_L$	0.64	0.44	0.30
	$\mathscr{D}_H$	0.60	0.51	0.32
	$\mathscr{D}_J$	0.84	0.89	0.35
Outcome B	$\mathscr{D}_L$	−0.77	−0.64	−0.59
	$\mathscr{D}_H$	−0.43	−0.31	−0.44
	$\mathscr{D}_J$	−0.74	−0.75	−0.61

(a) First seizure of patient I-2

Test		Before	During	After
Outcome A	$\mathscr{D}_L$	0.28	0.16	0.26
	$\mathscr{D}_H$	0.40	0.41	0.29
	$\mathscr{D}_J$	0.58	0.44	0.36
Outcome B	$\mathscr{D}_L$	−0.41	−0.23	−0.38
	$\mathscr{D}_H$	−0.29	−0.39	−0.27
	$\mathscr{D}_J$	−0.56	−0.54	−0.54

(b) All seizures across all patients

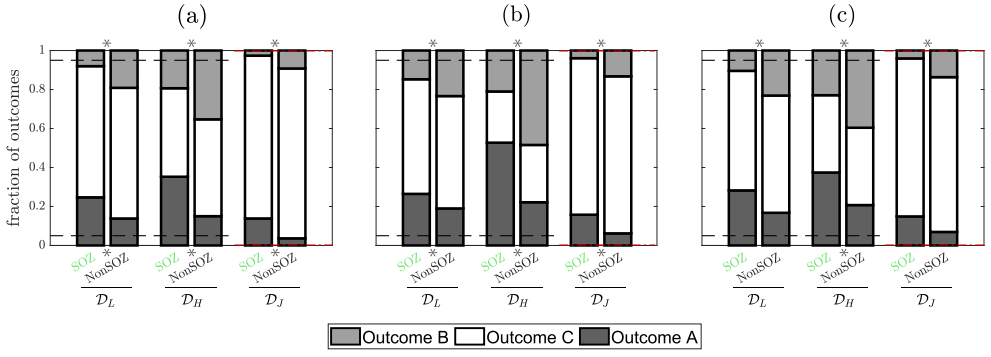

Fig. 5. Also across all seizures, for all three tests, outcome A is more frequent for SOZ channels, and outcome B is more frequent for nonSOZ channels. Same as Fig. 4 but here for the average across all seizures for all patients. Here, all fractions of outcomes are above the values to be expected under the null hypothesis H_0. In Table 2(b) we show the corresponding λ values. The asterisk ($*$) indicates p-value < 0.0056. That means the mean values used to calculate the λ values are significantly different according to a Wilcoxon signed-rank test (see Chapter 13.4 in Ref. Bluman, 2024). A Bonferroni correction for 9 comparisons (3 periods and 3 tests) was applied, using an initial significance level of 0.05. A Wilcoxon signed-rank test was used because normality was rejected for some of the distributions underlying the mean values, as assessed by the Kolmogorov–Smirnov test (see Chapter 6.2 in Ref. Bluman, 2024).

rows of Table 2(b), we expect $\lambda < 0$ in the majority of the cases. In fact, we have more seizures with $\lambda < 0$ for outcome B (Fig. 6(d)-(f)) than with $\lambda > 0$ for outcome A (Figs. 6(a)-(c)). Thus, nonSOZ channels reduce the network phase-locking in an even stronger way than SOZ channels enhance it. The database used in this study includes information on the type of epilepsy and the Engel Epilepsy Surgery Outcome Scale (see Table 1). While previous studies analysing this database found differences in the results between groups of patients with different surgical outcomes (Rummel et al. (2015); Goodfellow et al. (2016)), our analysis did not reveal any clear tendency in this regard. We also did not find any clear tendency with regard to the type of epilepsy. However, a bigger group of patients would be needed to test whether our results are influenced by the surgery outcome and/or the type of epilepsy.

4. Discussion

In this study, we introduce an approach to assess the phase-locking in functional EEG networks at the large-scale of the entire network as well as at the scale of individual network nodes. In a first step, we define the multivariate phase-locking measure from

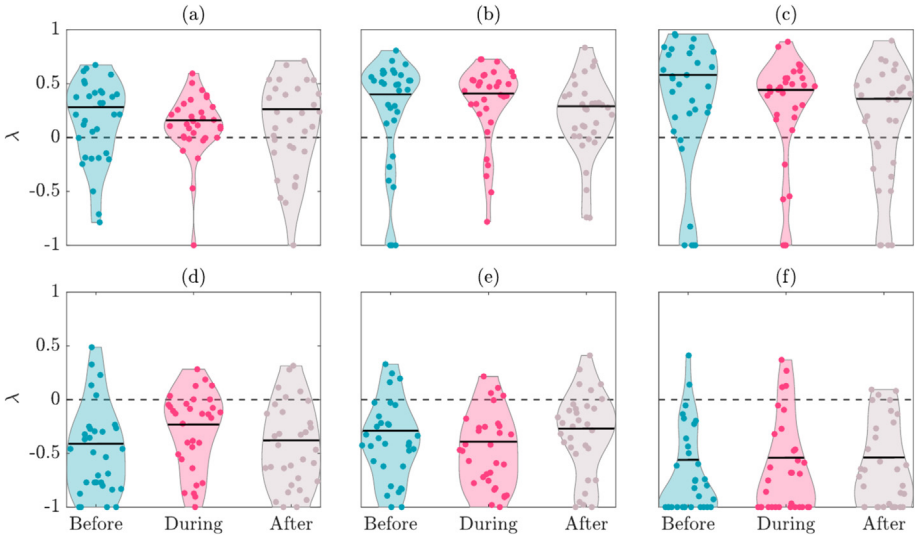

Fig. 6. The λ values from the thirty-two seizures from all sixteen patients confirm that, in general, SOZ nodes increase the network phase-locking, and nonSOZ nodes decrease it. Violin plots showing the distribution of the relative difference λ for the thirty-two seizures across different periods (before, during, and after seizure) and types of tests ($\mathscr{D}_L, \mathscr{D}_H$, and $\mathscr{D}_J$). Each dot represents one seizure and the area indicates the kernel density of the distribution. Black lines indicate the mean of all seizures, which correspond to the values shown in Table 2(b). (a) Relative difference λ for outcome A using the $\mathscr{D}_L$ test. (b) Same as (a) but using $\mathscr{D}_H$. (c) Same as (a) but using $\mathscr{D}_J$. (d) Relative difference λ for outcome B using $\mathscr{D}_L$. (e) Same as (d) but using $\mathscr{D}_H$. (f) Same as (d) but using $\mathscr{D}_J$.

the temporal average of the re-normalized mean resultant length (Andrzejak et al. (2023)). This allows us to quantify the overall phase-locking among all network nodes. In a second step, we assess the contribution of the individual network nodes to this phase-locking of the network. For this purpose, we compute the multivariate phase-locking for networks which are reduced by removing the signal of one node at a time. The difference between the multivariate phase-locking of the full and reduced networks allows us to determine phase-locking contribution of individual nodes. Finally, we use surrogate signals to determine if the phase-locking contribution results for the EEG signals are below or above the values which are expected for linear stochastic stationary correlated process. We apply this approach to peri-ictal EEG recordings of thirty-two seizures from sixteen patients. The signal measured with individual EEG channels is assumed to assess the dynamics of an individual node in a functional network. Overall, nodes in the seizure onset zone (SOZ) increase the large-scale phase-locking of the network. In contrast, nodes outside of this zone (nonSOZ) decrease the large-scale phase-locking. This is in line with earlier studies, which found that an elevated level of synchronization is related to the SOZ (Rijal et al. (2023); Espinoso and Andrzejak (2022); Andrzejak et al. (2012); Andrzejak et al. (2011); Mormann et al. (2000); Arnhold et al. (1999); Schevon et al. (2007); Ben-Jacob et al. (2007); Dauwels et al. (2009); Zaveri et al. (2009); Bettus et al. (2008); Rummel et al. (2010); Subramaniyam and Hyttinen (2015); Klimeš et al. (2015)).

In previous work, phase-locking is studied in pairs of EEG signals across time (Mormann et al. (2000); Espinoso and Andrzejak (2022); Bandarabadi et al. (2019); Leguia et al. (2021)) or across trials (Alnes et al. (2021); Mouraux and Iannetti (2008); Lachaux et al. (1999)). We here propose a complementary approach, combining a multivariate measure of phase-locking across EEG channels and a univariate measure of the phase-locking contribution of individual channels. The latter approach to assess the contribution of individual nodes to the large-scale network phase-locking has some analogy to the concept of sources and sinks in a network (Gunnarsdottir et al. (2022); Leguia et al. (2019)). The nodes identified as sources influence a set of neighboring nodes, while nodes identified as sinks are influenced by those source nodes. During ictal periods, Gunnarsdottir et al. observed that epileptogenic nodes become sources to propagate the seizure activity to other brain regions (Gunnarsdottir et al. (2022)). In our work, this corresponds to the increase of the network phase-locking by nodes in the SOZ. Studies using causality measures found that at high frequencies already in the preictal period, the signals registered from the SOZ are identified as causal sources (Epstein et al. (2014); Korzeniewska et al. (2014)). Additionally, through the use of information-theoretic measures, it was determined that the primary flow of information originates from focal sites (Sabesan et al. (2009); Paluš et al. (2001); Staniek and Lehnertz (2008); Leguia et al. (2019); Zubler et al. (2015)). In contrast, using Fokker-Plank coefficients Prusseit et al. found that the driving direction went from nonfocal to focal regions (Prusseit and Lehnertz (2008)).

Individual EEG channels might not fully capture sources and sinks of influence within the brain network. This aspect can be addressed because our method can readily be adapted to the scenario where sources and sinks are measured by groups of channels. The phase-locking contribution measure can be generalized by removing more than just one signal at a time. In an additional analysis, we created reduced networks by removing SOZ and nonSOZ signals as a group of nodes simultaneously. This approach is similar to that of Goodfellow et al. for the node ictogenicity measure (Goodfellow et al. (2016)) and to that of Schindler et al. for the correlation strength (Schindler et al. (2010)). We found that nodes in the seizure onset zone increased the network phase-locking also when considered group-wise (results not shown). For future work, it will be important to not only compare channels across the groups of SOZ and nonSOZ channels but also within each group. For example, one can compare nonSOZ channels located ipsi- and contralateral to the seizure onset zone. Furthermore, one can consider SOZ channels located on the same electrode or different electrodes.

Previous studies, which aim to find ways to improve postsurgical outcomes (Spencer et al. (2018); Taylor et al. (2018); Sinha et al. (2021)) analyzed how brain networks will be restructured after epilepsy surgery. One may consider comparing the analysis presented in this study and the hypothetical resection of a specific brain area. However, we cannot make this comparison. For the computation of the phase-locking contribution measure, only the

signals are excluded from the analysis. The structural connectivity among brain regions is evidently not affected by removing signals. Only in model systems, we would be able to remove a connection between nodes in the network. Thereby, we could assess whether the network undergoes a reorganization that redistributes the contributions of phase-locking.

As mentioned in the results section, breaking the results down with regard to the patients' Engel Epilepsy Surgery Outcome did not reveal any distinct tendency. However, the Engel classification can involve subjective elements, including self-reported seizure frequency and patient expectations, among others. Following the approach performed by Rummel et al. (2015), we applied our analysis to the overlap between SOZ channels and the channels located in brain regions that were surgically resected. It is important to note that these two channel categories do not necessarily coincide, as other clinical criteria can be considered when determining the brain areas to be resected. Nonetheless, we got similar results when using overlap between SOZ channels and the channels located in brain regions that were surgically resected instead of SOZ channels (not shown).

We selected our database to study the dynamics underlying signals registered directly before, during, and after the seizure. Future work should analyze long-term EEG data including extended seizure-free periods (Leguia et al. (2021); Le Van Quyen et al. (2005); Wang et al. (2018)). This will also allow studying the impact of interictal epileptiform discharges on the large-scale phase-locking, which may play an important role, even though they are a localized phenomenon both in time and space. One limitation of our study is the relatively small sample size, consisting of sixteen patients for which we analyzed a total of thirty-two perictal EEG recordings. More seizures were available (Table 1) but, as mentioned in the Materials and Methods section, we follow Refs. Rummel et al. (2015); Bandarabadi et al. (2019) and chose two seizures per patient to avoid over-representation of patients with many seizures. In our case, we employ the seizure pathway dissimilarity method (Schroeder et al. (2020); Schroeder et al. (2022)) to select the two seizures having the highest dissimilarity with regard to their spatiotemporal dynamics. In the Supplementary Material, we show some exemplary seizure pathways. It is important to mention that the two selected seizures represented well the diversity of the entire group of seizure pathways without including atypical seizures.

For band-pass filtering, we could have used the classical EEG frequency bands: $\delta, \theta, \alpha, \beta$, and γ. Instead, we opt for selecting the same filtering settings already used in Ref. Bandarabadi et al. (2019) since we were interested in analysing just one low (4–30 Hz) and one high (80–150 Hz) frequency range. Accordingly, we did not perform any in-sample tuning of these frequencies to optimize our results. Previous studies interested in cross-frequency coupling typically extract the phase of the HFOs envelope (Bandarabadi et al. (2019); Guirgis et al. (2015)). In contrast, we directly use the instantaneous Hilbert phase of the high-frequency oscillations. In future work one should study brain networks at different spatial scales. This can be done by including the signals of either all implanted electrodes to capture networks with long-range connections or of only a subset of electrodes to analyse local brain networks. This will allow testing if the multivariate phase-locking and phase-locking contributions of individual nodes in low and high frequencies are different for local versus long-range networks.

CRediT authorship contribution statement

Anaïs Espinoso: Conceptualization, Data curation, Resources, Methodology, Visualization, Software, Investigation, Formal analysis, Writing - original draft, Writing - review & editing. **Marc G. Leguia:** Methodology, Investigation, Formal analysis, Writing - original draft, Writing - review & editing. **Christian Rummel:** Data curation, Resources, Software, Writing - original draft, Writing - review & editing. **Kaspar Schindler:** Data curation, Resources, Software, Writing - original draft, Writing - review & editing. **Ralph. G. Andrzejak:** Conceptualization, Data curation, Methodology, Visualization, Investigation, Funding acquisition, Formal analysis, Writing - original draft, Writing - review & editing.

Declaration of Competing Interest

The authors declare that they have no known competing financial interests or personal relationships that could have appeared to influence the work reported in this paper.

Acknowledgements

A.E., R.G.A., and M.G.L. acknowledge funding from the Spanish Ministry of Science and Innovation and the State Research Agency (Grant No. PID2020-118196GBI00/MICIU/AEI/10.13039/501100011033). M.G.L. has been funded by the European Union-NextGenerationEU.

Appendix A. Results of three individual patients

We here provide additional examples for the outcomes of the joint test $\mathscr{D}_J$ for 3 different patients. The first case is the first seizure of patient IV-5, who belongs to the group of patients whose surgery did not lead to seizure freedom (Figs. A.7(a)-(d)). This seizure is a typical case that gives results similar to the patient average. The SOZ channels are all channels of the electrodes DER and IHPR, and the remaining channels from the other electrodes are nonSOZ channels. We can see that outcome A is mainly present in some SOZ channels and in the nonSOZ channels of electrode IHAR. Consequently, $\lambda_{J,\mathrm{A}}$ (Table A.3(a)) is positive and comparable to the values obtained for all patients (see first row of Table A.3 and again Table 2(b). The duration of this exemplary seizure is 14 s, which is substantially shorter than the average duration of all seizures included in the analysis (145.3 ± 37.1 s). This short duration, covering less than three consecutive analysis windows, may affect the results of the period during the seizure. With regard to outcome B, for the before period, it is obtained mainly in nonSOZ channels, with the exception of the IHAR electrode, and in some SOZ channels. Thus, a negative $\lambda_{J,\mathrm{B}}$ with high absolute value is observed for this period (Table A.3(b)). For the rest of the time periods, for test $\mathscr{D}_J$ outcome B is either absent or obtained only in nonSOZ channels, resulting in $\lambda_{J,\mathrm{B}} = -1$ (Fig. A.7 and Table A.3(b)).

The second example is the second seizure of patient II-5, who only had some disabling seizures post-surgery (Figs. A.7(e)-(h)). For this seizure, the signs of λ are partly different from the ones obtained from all patients, and overall the absolute values of λ are smaller. As compared with previous $\mathscr{D}_J$ examples, we observe mostly outcome C. Moreover, for test $\mathscr{D}_J$ outcome A is not predominant for SOZ channels, and outcome B is not predominant

for nonSOZ channels. Accordingly, for all three periods the obtained values of $\lambda_{J,A}$ and $\lambda_{J,B}$ are close to zero (Table A.3(a), (b)), and lower as compared with the mean values across all patients (Table 2(b)). Here we can see the importance of not only looking at λ values. During the seizure, we obtain $\lambda_{J,A}$ value of 0.27 for outcome A, despite an overall low rate of this outcome. It is therefore important to not only consider the relative differences λ but also the underlying fractions of rejections (Figs. 4, 5). For this exemplary case, the duration of the seizure is longer than the average duration of the rest of the included seizures (252 s vs 145.3 $\pm$ 37.1 s).

The last example is seizure one from patient IV-3, who did not become seizure-free after surgery (Figs. A.7(i)-(l)). In previous examples (Figs. 3(i)-(l), A.7(a)-(d), and A.7(e)-(h)), we mainly obtained positive $\lambda_{J,A}$ values and negative $\lambda_{J,B}$ values (Table 2(b)). In contrast, here SOZ channels never lead to outcome A of test $\mathscr{D}_J$. In contrast, nonSOZ channels lead to outcome A before, during, and after the seizure. Thus, here we obtain $\lambda_{J,A} = -1$ in all these periods (Table A.3(a)). Accordingly, results for this seizure of patient IV-3 are atypical since during the whole recording nonSOZ channels contribute more than SOZ channels to the network phase-locking. Concerning outcome B, recall that patient average $\lambda_{J,B}$ values are mainly negative (Table 2(b)). In this aspect, results for this seizure are not atypical since we obtain negative $\lambda_{J,B}$ values for all periods (Table A.3(b)). Out of all 49 channels, only 4 channels are classified as SOZ channels for this particular patient. Hence, any rejection taking place for these channels can play an important role in the computation of λ values. Furthermore, this patient provides another example of the importance of not only looking at λ values. For instance, in the after period for outcome B, $\lambda_{J,B}$ is near 0 with a fraction of rejection of $p_{\text{SOZ}} = 0.0833$ and $p_{\text{nonSOZ}} = 0.0840$.

Table A.3

Relative difference λ for the joint test $\mathscr{D}_J$ for three different patients. (a) λ values for outcome A of test $\mathscr{D}_J$. (b) Same as (a) but for outcome B.

Patient	Before	During	After	Patient	Before	During	After
All	0.58	0.44	0.36	All	−0.56	−0.54	−0.54
I-2	0.84	0.89	0.35	I-2	−0.74	−0.75	−0.61
IV-5	0.22	0.47	0.47	IV-5	−0.76	−1.00	−1.00
II-5	−0.10	0.27	0.15	II-5	−0.05	−0.09	0.09
IV-3	−1.00	−1.00	−1.00	IV-3	−0.17	−1.00	0.00
(a) Outcome A				(b) Outcome B			

Fig. A.7. Additional examples of test $\mathscr{D}_J$ for other patients. (a)–(d) Same as Fig. 3(i)–(l) but here for the first seizure of patient IV-5. This is a further typical example, for which results of the individual seizure are similar to the group average (Table 2(b) vs A.3). Channel labels are: DE, depth electrode; IHP, interhemispheric posterior; IHA, interhemispheric anterior; F, frontal; PL, parieto-lateral; accompanied by L or R if the electrodes are located in the left or right hemisphere, respectively. (e)–(h) Same as (a)–(d) but here for $\mathscr{D}_J$ test in the second seizure of patient II-5. This is an atypical example, for which absolute values of λ are low as compared to group results (Table 2(b) vs A.3). In particular, outcomes A or B are not found often for test $\mathscr{D}_J$ for any of the two channel categories. Channel labels are: FP, frontal-posterior; TP, temporo-posterior; TB, temporo-basal; ATPO, anterior temporo-polar; BTPO, baso-temporo-polar; FZ, fronto-central. (i)–(l) Same as (a)–(d) but here for $\mathscr{D}_J$ test in the first seizure of patient IV-3. This is an atypical example, for which λ values are different as compared to the group results (Table 2(b) vs A.3). In particular, outcome A is not found for the test $\mathscr{D}_J$ for SOZ channels in any of the periods. Channel labels are: TE, depth Electrode; TP, temporo-posterior; TBA, temporo-basal anterior; TBP, temporo-basal posterior; FOR1, fronto orbital 1; FOR2, fronto orbital 2; FP: fronto-polar.

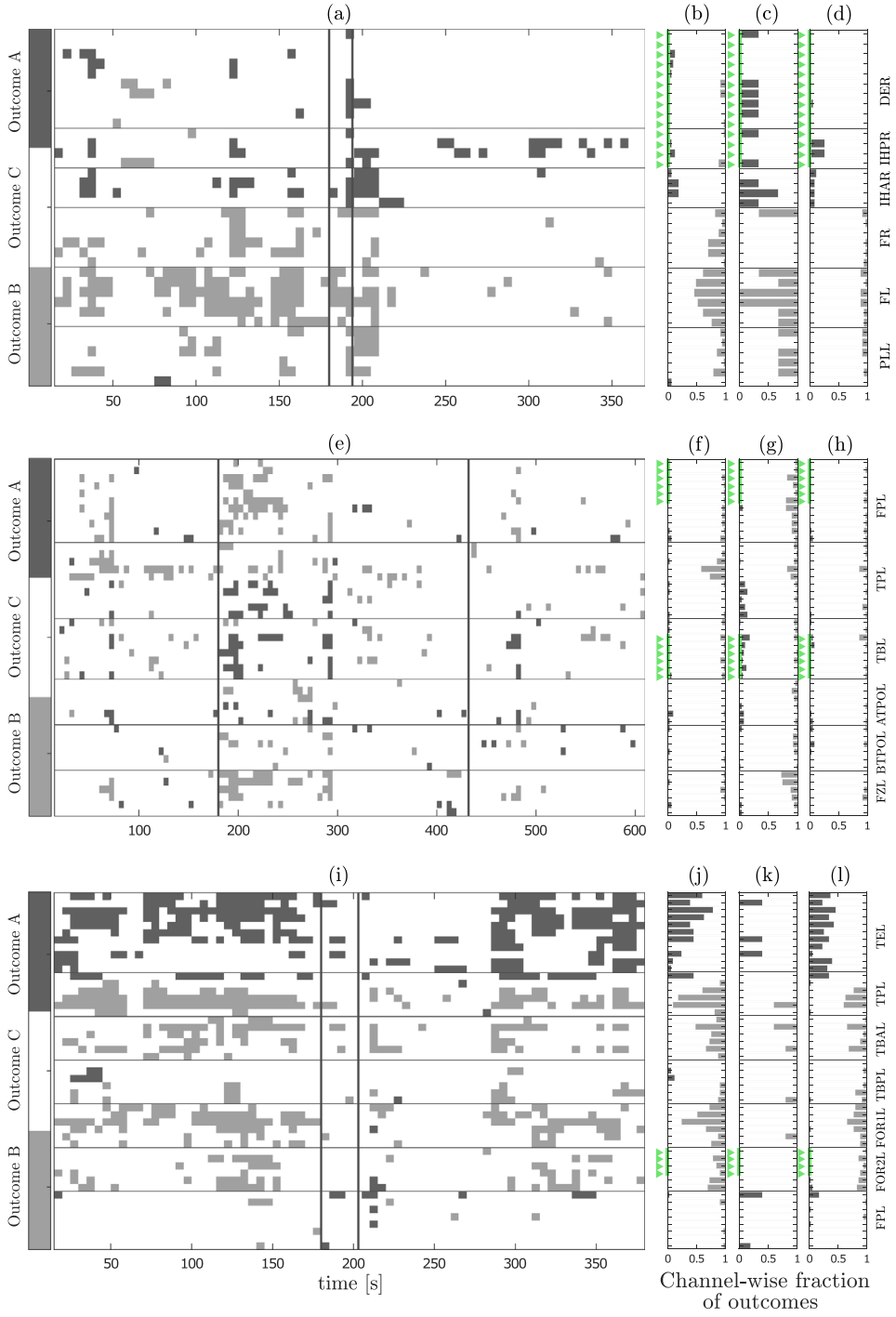

Appendix B. Supplementary material

Supplementary data associated with this article can be found, in the online version, at https://doi.org/10.1016/j.clinph.2024.09.008.

References

Achard S, Salvador R, Whitcher B, Suckling J, Bullmore E. A resilient, low-frequency, small-world human brain functional network with highly connected association cortical hubs. J Neurosci 2006;26: 63–72. publisher: Society for Neuroscience Section: Behavioral/Systems/Cognitive. URL: https://www.jneurosci.org/content/26/1/63, doi:10.1523/JNEUROSCI.3874-05.2006.

Alarcon G, Binnie CD, Elwes RDC, Polkey CE. Power spectrum and intracranial EEG patterns at seizure onset in partial epilepsy. Electroencephalogr Clin Neurophysiol 1995;94:326–37. https://doi.org/10.1016/0013-4694(94)00286-T.

Alnes SL, Lucia MD, Rossetti AO, Tzovara A. Complementary roles of neural synchrony and complexity for indexing consciousness and chances of surviving in acute coma. NeuroImage 2021;245:118638. https://doi.org/10.1016/j.neuroimage.2021.118638.

Andrzejak RG, Chicharro D, Lehnertz K, Mormann F. Using bivariate signal analysis to characterize the epileptic focus: the benefit of surrogates. Phys Rev E 2011;83:046203. https://doi.org/10.1103/PhysRevE.83.046203.

Andrzejak RG, Espinoso A, García-Portugués E, Pewsey A, Epifanio J, Leguia MG, et al. High expectations on phase locking: better quantifying the concentration of circular data. Chaos: An Interdiscip J Nonlinear Sci 2023;33: 091106, doi:10.1063/5.0166468. URL: doi: 10.1063/5.0166468.

Andrzejak RG, Kraskov A, Stögbauer H, Mormann F, Kreuz T. Bivariate surrogate techniques: necessity, strengths, and caveats. Phys Rev E 2003;68:066202. https://doi.org/10.1103/PhysRevE.68.066202.

Andrzejak RG, Schindler K, Rummel C. Nonrandomness, nonlinear dependence, and nonstationarity of electroencephalographic recordings from epilepsy patients. Phys Rev E 2012;86:046206. https://doi.org/10.1103/PhysRevE.86.046206.

Andrzejak RG, Widman G, Lehnertz K, Rieke C, David P, Elger CE. The epileptic process as nonlinear deterministic dynamics in a stochastic environment: an evaluation on mesial temporal lobe epilepsy. Epilepsy Res 2001;44:129–40. https://doi.org/10.1016/S0920-1211(01)00195-4.

Arnhold J, Grassberger P, Lehnertz K, Elger CE. A robust method for detecting interdependences: application to intracranially recorded EEG. Physica D 1999;134:419–30. https://doi.org/10.1016/S0167-2789(99)00140-2.

Bandarabadi M, Gast H, Rummel C, Bassetti C, Adamantidis A, Schindler K, et al. Assessing epileptogenicity using phase-locked high frequency oscillations: a systematic comparison of methods. Front Neurol 2019;10. URL: https://www.frontiersin.org/articles/10.3389/fneur.2019.01132.

Ben-Jacob E, Boccaletti S, Pomyalov A, Procaccia I, Towle VL. Detecting and localizing the foci in human epileptic seizures. Chaos: An Interdiscipl J Nonlinear Sci 2007;17: 043113, doi:10.1063/1.2805658. URL: doi: 10.1063/1.2805658.

Bettus G, Wendling F, Guye M, Valton L, Régis J, Chauvel P, et al. Enhanced EEG functional connectivity in mesial temporal lobe epilepsy. Epilepsy Res 2008;81:58–68. https://doi.org/10.1016/j.eplepsyres.2008.04.020.

Bluman A. Elementary statistics: a step by step approach, 11th edition Mc Graw Hill; 2024. URL: https://www.mheducation.com/highered/product/elementary-statistics-step-step-approach-bluman/M9781260360653.html.

Boccaletti S, Latora V, Moreno Y, Chavez M, Hwang DU. Complex networks: structure and dynamics. Phys Rep 2006;424:175–308. https://doi.org/10.1016/j.physrep.2005.10.009.

Brazier MAB. Spread of seizure discharges in epilepsy: anatomical and electrophysiological considerations. Exp Neurol 1972;36:263–72. https://doi.org/10.1016/0014-4886(72)90022-2.

Bröhl T, Lehnertz K. A perturbation-based approach to identifying potentially superfluous network constituents. Chaos: An Interdiscip J Nonlinear Sci 2023;33: 063119, doi:10.1063/5.0152030. URL: doi: 10.1063/5.0152030.

Bullmore E, Sporns O. Complex brain networks: graph theoretical analysis of structural and functional systems. Nat Rev Neurosci 2009;10:186–98. https://doi.org/10.1038/nrn2575.

Burns SP, Santaniello S, Yaffe RB, Jouny CC, Crone NE, Bergey GK, Anderson WS, Sarma SV. Network dynamics of the brain and influence of the epileptic seizure onset zone. Proc Nat Acad Sci 2014;111:E5321–30. https://doi.org/10.1073/pnas.1401752111.

Burrello A, Schindler K, Benini L, Rahimi A. Hyperdimensional computing with local binary patterns: one-shot learning of seizure onset and identification of ictogenic brain regions using short-time iEEG Recordings. IEEE Trans Biomed Eng 2020;67:601–13. https://doi.org/10.1109/TBME.2019.2919137.

Carreno M, Lüders HO General principles of pre-surgical evaluation. Textbook of epilepsy surgery. CRC Press; 2008.

Casdagli MC, Iasemidis LD, Savit RS, Gilmore RL, Roper SN, Chris Sackellares J. Non-linearity in invasive EEG recordings from patients with temporal lobe epilepsy. Electroencephalogr Clin Neurophysiol 1997;102:98–105. https://doi.org/10.1016/S0921-884X(96)95195-4.

Dauwels J, Eskandar E, Cash S. Localization of seizure onset area from intracranial non-seizure EEG by exploiting locally enhanced synchrony. In: 2009 Annual international conference of the IEEE engineering in medicine and biology society 2009;p. 2180–3. doi:10.1109/IEMBS.2009.5332447. iSSN: 1558-4615.

van Diessen E, Diederen SJH, Braun KPJ, Jansen FE, Stam CJ. Functional and structural brain networks in epilepsy: what have we learned? Epilepsia 2013;54:1855–65. https://doi.org/10.1111/epi.12350.

Engel Jr J. Outcome with respect to epileptic seizures. Surgical treatment of the epilepsies; 1993. 609–622. Publisher: Raven Press.

Epstein CM, Adhikari BM, Gross R, Willie J, Dhamala M. Application of high-frequency Granger causality to analysis of epileptic seizures and surgical decision making. Epilepsia 2014;55:2038–47. https://doi.org/10.1111/epi.12831.

Espinoso A, Andrzejak RG. Phase irregularity: a conceptually simple and efficient approach to characterize electroencephalographic recordings from epilepsy patients. Phys Rev E 2022;105:034212. https://doi.org/10.1103/PhysRevE.105.034212.

Espinoso A, Leguia MG, Rummel C, Schindler K, Andrzejak RG. [source code] Paper node contribution; 2024. URL: https://github.com/aespinoso/Espinoso_2024.git.

Fisher RS, Boas WvE, Blume W, Elger C, Genton P, Lee P, Engel Jr. J. Epileptic seizures and epilepsy: definitions proposed by the International League Against Epilepsy (ILAE) and the International Bureau for Epilepsy (IBE). Epilepsia 2005;46:470–2. https://doi.org/10.1111/j.0013-9580.2005.66104.x.

Gabor D. Theory of communication. Part 1: the analysis of information. J Inst Electr Eng - Part III: Radio Commun Eng 1946;93:429–41. https://doi.org/10.1049/ji-3-2.1946.0074.

Goodfellow M, Rummel C, Abela E, Richardson MP, Schindler K, Terry JR. Estimation of brain network ictogenicity predicts outcome from epilepsy surgery. Sci Rep 2016;6:29215. https://doi.org/10.1038/srep29215.

Guirgis M, Chinvarun Y, Campo Md, Carlen PL, Bardakjian BL. Defining regions of interest using cross-frequency coupling in extratemporal lobe epilepsy patients. J Neural Eng 2015;12:026011. https://doi.org/10.1088/1741-2560/12/2/026011.

Gunnarsdottir KM, Li A, Smith RJ, Kang JY, Korzeniewska A, Crone NE, Rouse AG, Cheng JJ, Kinsman MJ, Landazuri P, Uysal U, Ulloa CM, Cameron N, Cajigas I, Jagid J, Kanner A, Elarjani T, Bicchi MM, Inati S, Zaghloul KA, Boerwinkle VL, Wyckoff S, Barot N, Gonzalez-Martinez J, Sarma SV. Source-sink connectivity: a novel interictal EEG marker for seizure localization. Brain 2022;145:3901–15. https://doi.org/10.1093/brain/awac300.

Honey CJ, Sporns O. Dynamical consequences of lesions in cortical networks. Hum Brain Mapp 2008;29:802–9. https://doi.org/10.1002/hbm.20579.

Imamura H, Matsumoto R, Inouchi M, Matsuhashi M, Mikuni N, Takahashi R, Ikeda A. Ictal wideband ECoG: direct comparison between ictal slow shifts and high frequency oscillations. Clin Neurophysiol 2011;122:1500–4. https://doi.org/10.1016/j.clinph.2010.12.060.

Jacobs J, Zijlmans M, Zelmann R, Chatillon C, Hall J, Olivier A, Dubeau F, Gotman J. High-frequency electroencephalographic oscillations correlate with outcome of epilepsy surgery. Annals Neurol 2010;67:209–20. https://doi.org/10.1002/ana.21847.

Kaiser M, Martin R, Andras P, Young MP. Simulation of robustness against lesions of cortical networks. Eur J Neurosci 2007;25:3185–92. https://doi.org/10.1111/j.1460-9568.2007.05574.x.

Khambhati AN, Davis KA, Oommen BS, Chen SH, Lucas TH, Litt B, Bassett DS. Dynamic network drivers of seizure generation, propagation and termination in human neocortical epilepsy. PLOS Comput Biol 2015;11:e1004608. https://doi.org/10.1371/journal.pcbi.1004608.

Klimeš P, Duque JJ, Jurák P, Halámek J, Worrell GA. Connectivity of epileptic brain regions in wake and sleep. In: 2015 37th Annual international conference of the IEEE engineering in medicine and biology society (EMBC);2015. p. 2191–4. doi:10.1109/EMBC.2015.7318825. iSSN: 1558-4615.

Korzeniewska A, Cervenka MC, Jouny CC, Perilla JR, Harezlak J, Bergey GK, Franaszczuk PJ, Crone NE. Ictal propagation of high frequency activity is recapitulated in interictal recordings: effective connectivity of epileptogenic networks recorded with intracranial EEG. NeuroImage 2014;101:96–113. https://doi.org/10.1016/j.neuroimage.2014.06.078.

Kramer MA, Cash SS. Epilepsy as a disorder of cortical network organization. The Neuroscientist 2012;18:360–72. https://doi.org/10.1177/1073858411422754.

Kramer MA, Eden UT, Kolaczyk ED, Zepeda R, Eskandar EN, Cash SS. Coalescence and fragmentation of cortical networks during focal seizures. J Neurosci 2010;30:10076–85. https://doi.org/10.1523/JNEUROSCI.6309-09.2010.

Kramer MA, Kolaczyk ED, Kirsch HE. Emergent network topology at seizure onset in humans. Epilepsy Res 2008;79:173–86. https://doi.org/10.1016/j.eplepsyres.2008.02.002.

Krucoff MO, Chan AY, Harward SC, Rahimpour S, Rolston JD, Muh C, Englot DJ. Rates and predictors of success and failure in repeat epilepsy surgery: a meta-analysis and systematic review. Epilepsia 2017;58:2133–42. https://doi.org/10.1111/epi.13920.

Kuramoto Y. Chemical oscillations, waves, and turbulence. volume 19 of Springer Series in Synergetics. Springer, Berlin, Heidelberg; 1984. doi:10.1007/978-3-642-69689-3. URL: http://link.springer.com/10.1007/978-3-642-69689-3.

Lachaux JP, Rodriguez E, Martinerie J, Varela FJ. Measuring phase synchrony in brain signals. Hum. Brain Mapp 1999;8:194–208. https://doi.org/10.1002/(SICI)1097-0193(1999)8:4<194::AID-HBM4>3.0.CO;2-C.

Le Van Quyen M, Soss J, Navarro V, Robertson R, Chavez M, Baulac M, Martinerie J. Preictal state identification by synchronization changes in long-term intracranial EEG recordings. Clin Neurophysiol 2005;116:559–68. https://doi.org/10.1016/j.clinph.2004.10.014.

Leguia MG, Martínez CGB, Malvestio I, Campo AT, Rocamora R, Levnajić Z, Andrzejak RG. Inferring directed networks using a rank-based connectivity measure. Phys Rev E 2019;99:012319. https://doi.org/10.1103/PhysRevE.99.012319.

Leguia MG, Rao VR, Kleen JK, Baud MO. Measuring synchrony in bio-medical timeseries. Chaos: An Interdiscip J Nonlinear Sci 2021;31:013138, doi:10.1063/5.0026733. URL: doi: 10.1063/5.0026733.
Lehnertz K, Ansmann G, Bialonski S, Dickten H, Geier C, Porz S. Evolving networks in the human epileptic brain. Physica D 2014;267:7–15. https://doi.org/10.1016/j.physd.2013.06.009.
Mardia KV, Jupp PE. Directional statistics. volume 2. Wiley Online Library; 2000.
Modur PN, Vitaz TW, Zhang S. Seizure localization using broadband EEG: comparison of conventional frequency activity, high-frequency oscillations, and infraslow activity. J Clin Neurophysiol: Off Publicat Am Electroencephalogr Soc 2012;29:309–19. https://doi.org/10.1097/WNP.0b013e318262435d.
Mormann F, Kreuz T, Andrzejak RG, David P, Lehnertz K, Elger CE. Epileptic seizures are preceded by a decrease in synchronization. Epilepsy Res 2003;53:173–85. https://doi.org/10.1016/S0920-1211(03)00002-0.
Mormann F, Lehnertz K, David P, Elger EC. Mean phase coherence as a measure for phase synchronization and its application to the EEG of epilepsy patients. Phys D: Nonlinear Phenom 2000;144: 358–69, doi:10.1016/S0167-2789(00)00087-7. URL: https://www.sciencedirect.com/science/article/pii/S0167278900000877.
Mouraux A, Iannetti GD. Across-trial averaging of event-related EEG responses and beyond. Magn Reson Imag 2008;26:1041–54. https://doi.org/10.1016/j.mri.2008.01.011.
Ortega GJ, Menendez de la Prida L, Sola RG, Pastor J. Synchronization clusters of interictal activity in the lateral temporal cortex of epileptic patients: intraoperative electrocorticographic analysis. Epilepsia 2008;49:269–80. https://doi.org/10.1111/j.1528-1167.2007.01266.x.
Osterhage H, Mormann F, Staniek M, Lehnertz K. Measuring synchronization in the epileptic brain: a comparison of different approaches. Int J Bifurc Chaos 2007;17:3539–44. https://doi.org/10.1142/S0218127407019330.
Paluš M, Komárek V, Hrnčíř Z, Štěrbová K. Synchronization as adjustment of information rates: detection from bivariate time series. Phys Rev E 2001;63:046211. https://doi.org/10.1103/PhysRevE.63.046211.
Penfield W, Jasper H Epilepsy and the functional anatomy of the human brain. Epilepsy and the functional anatomy of the human brain. Oxford, England: Little, Brown & Co; 1954.
Pijn JP, Van Neerven J, Noest A, Lopes da Silva FH. Chaos or noise in EEG signals; dependence on state and brain site. Electroencephalogr Clin Neurophysiol 1991;79:371–81. https://doi.org/10.1016/0013-4694(91)90202-F.
Pijn JPM, Vijn PCM, Lopes da Silva FH, Van Ende Boas W, Blanes W. Localization of epileptogenic foci using a new signal analytical approach. Neurophysiol Clin/Clin Neurophysiol 1990;20:1–11. https://doi.org/10.1016/S0987-7053(05)80165-0.
Ponten SC, Bartolomei F, Stam CJ. Small-world networks and epilepsy: graph theoretical analysis of intracerebrally recorded mesial temporal lobe seizures. Clin Neurophysiol 2007;118:918–27. https://doi.org/10.1016/j.clinph.2006.12.002.
Prichard D, Theiler J. Generating surrogate data for time series with several simultaneously measured variables. Phys Rev Lett 1994;73:951–4. https://doi.org/10.1103/PhysRevLett.73.951.
Prusseit J, Lehnertz K. Measuring interdependences in dissipative dynamical systems with estimated Fokker-Planck coefficients. Phys Rev E 2008;77:041914. https://doi.org/10.1103/PhysRevE.77.041914.
Quian Quiroga R, Kraskov A, Kreuz T, Grassberger P. Performance of different synchronization measures in real data: a case study on electroencephalographic signals. Phys Rev E 2002;65:041903. https://doi.org/10.1103/PhysRevE.65.041903.
Rijal S, Corona L, Perry MS, Tamilia E, Madsen JR, Stone SSD, Bolton J, Pearl PL, Papadelis C. Functional connectivity discriminates epileptogenic states and predicts surgical outcome in children with drug resistant epilepsy. Scient Rep 2023;13:9622. https://doi.org/10.1038/s41598-023-36551-0.
Rosenow F, Lüders H. Presurgical evaluation of epilepsy. Brain 2001;124:1683–700. https://doi.org/10.1093/brain/124.9.1683.
Rummel C, Abela E, Andrzejak RG, Hauf M, Pollo C, Müller M, Weisstanner C, Wiest R, Schindler K. Resected brain tissue, seizure onset zone and quantitative EEG measures: towards prediction of post-surgical seizure control. PLOS ONE 2015;10:e0141023. https://doi.org/10.1371/journal.pone.0141023.
Rummel C, Baier G, Müller M. The influence of static correlations on multivariate correlation analysis of the EEG. J Neurosci Methods 2007;166:138–57. https://doi.org/10.1016/j.jneumeth.2007.06.023.
Rummel C, Müller M, Baier G, Amor F, Schindler K. Analyzing spatio-temporal patterns of genuine cross-correlations. J Neurosci Methods 2010;191:94–100. https://doi.org/10.1016/j.jneumeth.2010.05.022.
Sabesan S, Good LB, Tsakalis KS, Spanias A, Treiman DM, Iasemidis LD. Information flow and application to epileptogenic focus localization from intracranial EEG. IEEE Trans Neural Syst Rehabil Eng 2009;17, 244–253. doi:10.1109/TNSRE.2009.2023291. conference Name: IEEE Transactions on Neural Systems and Rehabilitation Engineering.
Schevon CA, Cappell J, Emerson R, Isler J, Grieve P, Goodman R, Mckhann G, Weiner H, Doyle W, Kuzniecky R, Devinsky O, Gilliam F. Cortical abnormalities in epilepsy revealed by local EEG synchrony. NeuroImage 2007;35:140–8. https://doi.org/10.1016/j.neuroimage.2006.11.009.
Schindler K, Amor F, Gast H, Müller M, Stibal A, Mariani L, Rummel C. Peri-ictal correlation dynamics of high-frequency (80–200Hz) intracranial EEG. Epilepsy Res 2010;89:72–81. https://doi.org/10.1016/j.eplepsyres.2009.11.006.
Schindler KA, Bialonski S, Horstmann MT, Elger CE, Lehnertz K. Evolving functional network properties and synchronizability during human epileptic seizures. Chaos: An Interdiscip J Nonlinear Sci 2008;18: 033119, doi:10.1063/1.2966112. publisher: American Institute of Physics. URL: https://aip.scitation.org/doi/full/10.1063/1.2966112.
Schreiber T, Schmitz A. Improved surrogate data for nonlinearity tests. Phys Rev Lett 1996;77:635–8. https://doi.org/10.1103/PhysRevLett.77.635.
Schreiber T, Schmitz A. Surrogate time series. Physica D 2000;142:346–82. https://doi.org/10.1016/S0167-2789(00)00043-9.
Schroeder GM, Chowdhury FA, Cook MJ, Diehl B, Duncan JS, Karoly PJ. Multiple mechanisms shape the relationship between pathway and duration of focal seizures. Brain Commun 2022;4: fcac173, doi:10.1093/braincomms/fcac173. URL: doi: 10.1093/braincomms/fcac173.
Schroeder GM, Diehl B, Chowdhury FA, Duncan JS, de Tisi J, Trevelyan AJ, Forsyth R, Jackson A, Taylor PN, Wang Y. Seizure pathways change on circadian and slower timescales in individual patients with focal epilepsy. Proc Nat Acad Sci 2020;117:11048–58. https://doi.org/10.1073/pnas.1922084117.
Sinha N, Joshi RB, Sandhu MRS, Netoff TI, Zaveri HP, Lehnertz K. Perspectives on understanding aberrant brain networks in epilepsy. Front Network Physiol 2022;2. URL: https://www.frontiersin.org/articles/10.3389/fnetp.2022.868092.
Sinha N, Wang Y, Silva NMd, Miserocchi A, McEvoy AW, Tisi Jd, Vos SB, Winston GP, Duncan JS, Taylor PN. Structural brain network abnormalities and the probability of seizure recurrence after epilepsy surgery. Neurology 2021;96: e758–71. https://doi.org/10.1212/WNL.0000000000011315.
Spencer DD, Gerrard JL, Zaveri HP. The roles of surgery and technology in understanding focal epilepsy and its comorbidities. The Lancet Neurol 2018;17:373–82. https://doi.org/10.1016/S1474-4422(18)30031-0.
Spencer S, Huh L. Outcomes of epilepsy surgery in adults and children. The Lancet Neurol 2008;7:525–37. https://doi.org/10.1016/S1474-4422(08)70109-1.
Spencer SS. Neural networks in human epilepsy: evidence of and implications for treatment. Epilepsia 2002;43:219–27. https://doi.org/10.1046/j.1528-1157.2002.26901.x.
Stam CJ, Nolte G, Daffertshofer A. Phase lag index: assessment of functional connectivity from multi channel EEG and MEG with diminished bias from common sources. Hum Brain Mapp 2007;28:1178–93. https://doi.org/10.1002/hbm.20346.
Staniek M, Lehnertz K. Symbolic transfer entropy. Phys Rev Lett 2008;100:158101. https://doi.org/10.1103/PhysRevLett.100.158101.
Subramaniyam NP, Hyttinen J. Dynamics of intracranial electroencephalographic recordings from epilepsy patients using univariate and bivariate recurrence networks. Phys Rev E 2015;91:022927. https://doi.org/10.1103/PhysRevE.91.022927.
Taylor PN, Sinha N, Wang Y, Vos SB, de Tisi J, Miserocchi A, et al. The impact of epilepsy surgery on the structural connectome and its relation to outcome. NeuroImage: Clin 2018;18: 202–14, doi:10.1016/j.nicl.2018.01.028. URL: https://www.sciencedirect.com/science/article/pii/S2213158218300287.
Theiler J, Eubank S, Longtin A, Galdrikian B, Doyne Farmer J. Testing for nonlinearity in time series: the method of surrogate data. Physica D 1992;58:77–94. https://doi.org/10.1016/0167-2789(92)90102-S.
Wang D, Ren D, Li K, Feng Y, Ma D, Yan X, Wang G. Epileptic seizure detection in long-term EEG recordings by using wavelet-based directed transfer function. IEEE Trans Biomed Eng 2018;65:2591–9. https://doi.org/10.1109/TBME.2018.2809798.
Weiss SA, Lemesiou A, Connors R, Banks GP, McKhann GM, Goodman RR, Zhao B, Filippi CG, Nowell M, Rodionov R, Diehl B, McEvoy AW, Walker MC, Trevelyan AJ, Bateman LM, Emerson RG, Schevon CA. Seizure localization using ictal phase-locked high gamma: a retrospective surgical outcome study. Neurology 2015;84:2320–8. https://doi.org/10.1212/WNL.0000000000001656.
Wendling F, Bartolomei F, Bellanger JJ, Chauvel P. Interpretation of interdependencies in epileptic signals using a macroscopic physiological model of the EEG. Clin Neurophysiol 2001;112:1201–18. https://doi.org/10.1016/S1388-2457(01)00547-8.
Wu S, Kunhi Veedu HP, Lhatoo SD, Koubeissi MZ, Miller JP, Lüders HO. Role of ictal baseline shifts and ictal high-frequency oscillations in stereo-electroencephalography analysis of mesial temporal lobe seizures. Epilepsia 2014;55:690–8. https://doi.org/10.1111/epi.12608.
Zaveri HP, Pincus SM, Goncharova II, Duckrow RB, Spencer DD, Spencer SS. Localization-related epilepsy exhibits significant connectivity away from the seizure-onset area. NeuroReport 2009;20:891. https://doi.org/10.1097/WNR.0b013e32832c78e0.
Zijlmans M, Jiruska P, Zelmann R, Leijten FS, Jefferys JG, Gotman J. High-frequency oscillations as a new biomarker in epilepsy. Annals Neurol 2012;71:169–78. https://doi.org/10.1002/ana.22548.
Zubler F, Gast H, Abela E, Rummel C, Hauf M, Wiest R, Pollo C, Schindler K. Detecting functional hubs of ictogenic networks. Brain Topogr 2015;28:305–17. https://doi.org/10.1007/s10548-014-0370-x.